UC Irvine
UC Irvine Previously Published Works

Title
Dual-frequency interferometric SAR observations of a tropical rain-forest

Permalink
https://escholarship.org/uc/item/3w10k2fx

Journal
Geophysical Research Letters, 23(9)

ISSN
0094-8276

Author
Rignot, E

Publication Date
1996-05-01

DOI
10.1029/96gl00456

Copyright Information

Peer reviewed

Dual-frequency interferometric SAR observations of a tropical rain-forest

E. Rignot

Jet Propulsion Laboratory, California Institute of Technology, Pasadena, CA

Abstract. Repeat-pass, interferometric, radar observations of tropical rain-forest collected by the Shuttle Imaging Radar C (SIR-C) in the state of Rondonia, Brazil, reveal signal coherence is destroyed at C-band (5.6-cm) in the forest, whereas L-band (24-cm) radar signals remain strongly coherent over the entire landscape. At L-band, the rms difference in inferred topographic height between the forest and adjacent clearings is 5 m, equivalent to the height noise. Atmospheric delays are large, however, forming kilometer-sized anomalies with a 1.2-cm rms one way. Radar interferometric studies of the humid tropics must therefore be conducted at long radar wavelengths, with kilometric baselines or with two antennas operating simultaneously.

Introduction

The recent advent of synthetic-aperture radar (SAR) interferometry to map the surface topography of land surfaces and to detect wavelength-sized changes in surface topography caused by natural events has stirred interest for this technique in the scientific community. Surface topography of our planet is poorly known, especially in the tropics where digital topographic maps are seldomly available, and SAR interferometry may offer the only promise to provide self-consistent, global, topographic maps (Zebker et al., 1994).

Knowing surface topography is important for studying forested ecosystems. Elevation, slope and aspect exert control on intercepted solar radiation, precipitation and runoff, river flooding, evaporation, soil moisture and vegetation type and health. Slope and aspect in digital form are also required for calibrating remote sensing satellite imagery.

Most results obtained to date with radar interferometry have utilized data collected by the European ERS-1 satellite which operates a C-band frequency (5.6 cm wavelength) radar with vertical transmit and receive polarization. Over desert areas and polar ice sheets, the signal remains coherent from several days up to several years, and radar interferometry works well. Over vege-

tated terrain, the temporal coherence of the SAR signal worsens considerably, especially over forests (Hagberg et al., 1995), and radar interferometry is less practical.

The Shuttle Imaging Radar C (SIR-C) experiment provided the first opportunity to compare the merits and values of C- and L-band frequencies for repeat-pass radar interferometry applications over land. SIR-C collected interferometric data at a one-day repeat-pass cycle during the last few days of its second mission, covering large areas in the tropics. The images analyzed here were acquired at 10.61° south, 63.51° west, south of the city of Porto Velho and west of the city of Ariquemes, in the state of Rondonia, Brazil, on October 7, 8 and 9, 1994, during orbit 119, 135 and 151 of the space shuttle Endeavour. The radar image shown in Figure 1 (orbit 119) is 46.1 km x 34.3 km in size, with the radar flying from left to right, looking to its left, 208 km above ground. The angle of the radar illumination with the horizontal is $\theta = 45.2°$. Spatial resolution is $R_r = 44$ m in range and $R_z = 49$ m in azimuth (along-track) after spatial averaging using 6 samples in range and 6 samples in azimuth. Radar images were acquired simultaneously at L- (24 cm) and C-band (5.6 cm) frequencies, with vertical transmit and receive linear polarization.

The state of Rondonia had deforestation in the 1970's and 1980's documented by optical sensors (Tucker et al., 1984). Large areas of tropical forests are cleared every year to yield new pasture for raising cattle and subsidence cultivations. Cleared areas generally appear dark in radar images due to their low backscatter intensity, and are located along or close to roads.

Methods

As all modern SARs, the SIR-C instrument recorded the signal amplitude and phase of the radar returns expressed as a complex number for each image pixel. Images gathered during repeat-passes of the shuttle along the exact same orbit were co-registered with sub-pixel precision using the correlation of the signal intensity. The registered data were utilized to compute the normalized cross-correlation coefficient of the complex amplitudes measured by the radar on two different dates. The magnitude of this coefficient, ρ, measures the temporal coherence of the SAR signal between 0 (no coherence) and 1 (perfect coherence). Its phase, ϕ, is the interferometric phase which measures the relative displacement of the surface element along the radar line of
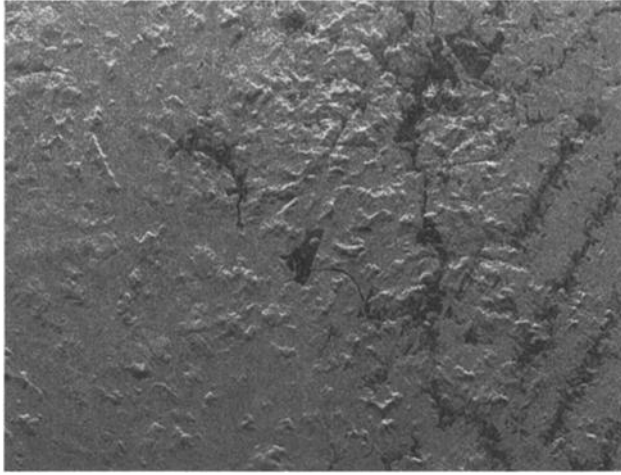
Figure 1. L-band (24-cm wavelength) radar image of a test site in Rondonia, Brazil. Image size is 46.1 km x 34.3 km, resolution is 40 m.

sight between the two instances of imaging.

The temporal coherence image of the pair combining orbit 119 and 135 is shown in Figure 2 at L- and C-band. A similar image was obtained for the data acquired during orbit 135 and 151. L-band coherence is high for the forest ($\rho > 0.7$) and clearings ($\rho > 0.85$). C-band coherence is high for clearings ($\rho > 0.6$) but low for the forest ($\rho < 0.2$).

A height map obtained from the first pair of SIR-C images is shown in Figure 3. We estimated the baseline separation between the successive positions of the radar antenna in the least square sense, using 50 tie-points from a published topographic map at 1:100,000. Tie-points were selected on hill tops, roads or rivers easy to identify in both the printed map and the digital SAR imagery. Between the first two passes, the baseline separation was $B = 230$ m, with an orientation angle $\alpha = - 27°$ above horizontal, corresponding to a baseline component perpendicular to the radar illumination $B_\perp = B \sin (\alpha + \theta)$ equal to 72 m, slowly varying along-track. For the second pair, B was 114 m and α was +82.4°, yielding $B_\perp = 90$ m.

Sources of Coherence Reduction

Factors influencing signal coherence may be separated into two categories: 1) system effects, and 2) surface effects. System effects include: 1) thermal noise, and 2) geometric coherence reductions. These error sources are independent, and their effect on temporal coherence is multiplicative (Zebker and Villasenor, 1992). For thermal noise, the multiplicative coherence coefficient is

$$\rho_{SNR} = (1 + SNR^{-1})^{-1}, \qquad (1)$$

where SNR is the signal-to-noise ratio. System noise was estimated from the signal intensity measured in the

darkest portions of the radar scene, meaning open water and regions shadowed from the radar illumination. The resulting SNR was 12 and 18 dB at L-band for the forest and for clearings, respectively, and 16 dB and 20 dB at C-band, yielding $\rho_{SNR} > 0.94$.

Geometric coherence reduction occurs when the line of sights from the centers of the synthetic apertures to a pixel point in different directions during successive passes. When the plane of incidence of the radar illumination is the same in both passes, the geometric coherence reduction is

$$\rho_B = 1 - 2 \lambda^{-1} R^{-1} B_\perp R_r \sin^2 (\theta) \qquad (2)$$

where R is the distance from the radar antenna to a pixel. With $R = 287$ km and $B_\perp = 72$ m, we find ρ_B is 0.95 at L-band and 0.80 at C-band.

When the plane of incidence of the radar illumination rotates by an angle $\Delta\psi$ in the horizontal plane between successive passes, coherence is further reduced because $\Delta\psi$ introduces a doppler shift in the data. Modeling the impulse response of the SAR signal as a sin(x)/(x) function, the corresponding coherence reduction is

$$\rho_\psi = 1 - 2 \lambda^{-1} R_z \Delta\psi \qquad (3)$$

The squint angles, ψ's, are estimated very precisely during SAR processing. The results yield $\rho_\psi > 0.96$ at L-band and $\rho_\psi > 0.81$ at C-band for both image pairs.

Combined together, these system effects reduce signal coherence by 8 to 21%. We conclude the lack of coherence over forests observed at C-band is not a system effect but a surface effect.

A surface effect means a change in the nature and spatial distribution of the scatterers responsible for the measured radar returns in between successive passes. At C-band, theoretical models and experimental evidence have shown that radar scattering is dominated by contributions from the smaller branches, twigs and needles or leaves of the upper canopy (e.g. Beaudoin et al., 1994). Random agitations in the position of small branches, twigs and leaves, for instance induced by wind, are therefore likely to reduce signal coherence because they will change the spatial distribution of the scatterers. One situation where wind influence may not affect the temporal coherence of the SAR signal is when the forest is frozen. In that case, the dielectric constant of woody and leafy material is low, attenuation of the
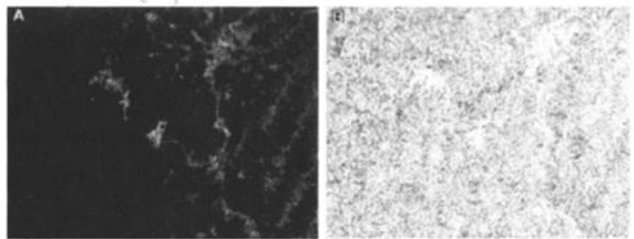

Figure 2. Temporal coherence of image pair 119/135 at (A) C- and (B) L-band frequency. High correlation is bright, low correlation is dark.
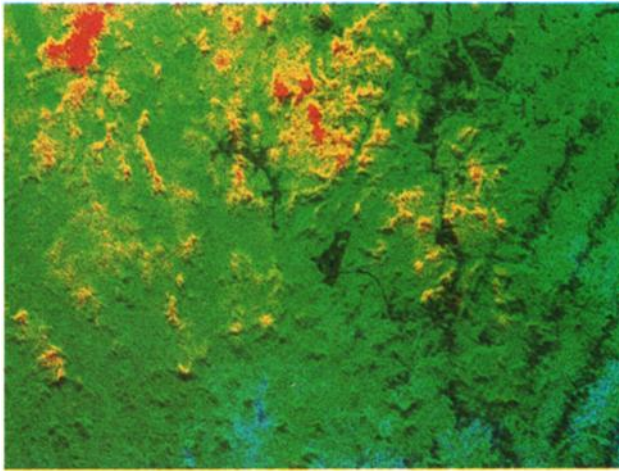
Figure 3. Elevation map derived from the L-band data. Hue and saturation are proportional to the inverse of the height, and intensity is proportional to the radar brightness at L-band. Terrain height ranges from 200 to 600 m.

radar signals is reduced, and the upper canopy conditions play a less critical role in radar scattering. As a result, $\rho > 0.5$ in winter over boreal forests of northern Europe with ERS-1 SAR (Hagberg et al., 1995).

At L-band, the radar signals penetrate deeper into the forest canopy and interact with the larger-sized forest constituents such as large branches and tree-trunks, and the ground. The larger objects and the ground are less subject to random fluctuations in position, explaining why signal coherence remains higher at L-band.

Topographic mapping at L-band

Height errors include uncertainties in range distance due to system clock timing, data sampling clock jitter or atmospheric propagation delays, system attitude and baseline separation, altitude of the spacecraft, and phase noise (Li and Goldstein, 1990). In examining lo-
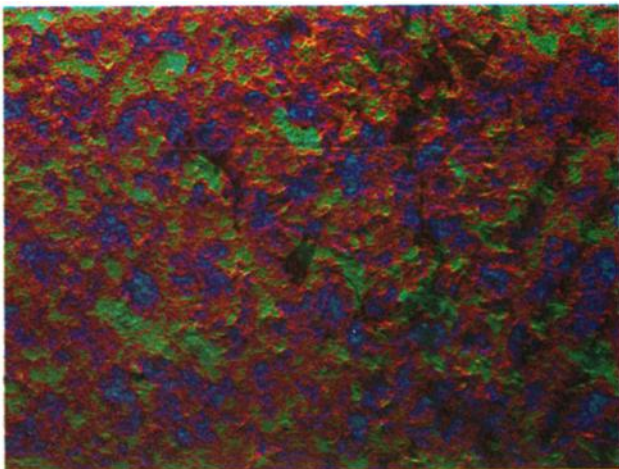
cal variations in surface height, however, height errors are dominated by phase noise and range delays through the atmosphere and the forest canopy. The uncertainty in terrain height, σ_h, caused by phase noise, σ_ϕ, is

$$\sigma_h = \lambda (4\pi)^{-1} R \cos \theta \, B_\perp^{-1} \sigma_\phi \quad (4)$$

$$\text{where,} \quad \sigma_\phi = N^{-\frac{1}{2}} \rho^{-1} \sqrt{1 - \rho} \quad (5)$$

where $N = 36$ is the number of looks of the data. For clearings, $\rho = 0.85$ yields $\sigma_\phi = 4°$ and $\sigma_h = 5$ m. For the forest, $\rho = 0.7$ and $\sigma_h = 8$ m.

As radar signals penetrate the forest canopy, they interact with a medium of dielectric constant greater than for air, increasing the electrical path length compared to that for clearings. Here, woody biomass is 350 kg/m^2 (Fearnside et al., 1992), wood density is 690 kg m^{-3} (Brown and Lugo, 1992) and tree height is h = 30 m (Grace et al., 1995). Wood occupies 0.17% of the forest volume. With a dielectric constant of 20 for wood/leaves and 1 for air, van Beek (1967)'s mixing formula yields a dielectric constant of 1.01 for the forest. The one-way increase in electrical path length is 0.01 h sin(θ) or 26 cm, much less than phase noise.

Following Goldstein (1995), we estimated the atmospheric propagation delays by fitting a quadratic function through the phase data obtained from two interferograms. The residual phase disturbances are shown in Figure 4, scaled between -3 cm and +3 cm one-way range delay. The rms error in electrical path length is 1.2 cm, 5 times larger than observed in the California desert (Goldstein, 1995). Larger values were expected in the more humid conditions of tropical rain-forests since these atmospheric delays are attributed to turbulent water vapor mixing. With $B_\perp = 72$ m, these range delays translate into 35 m uncertainties in surface height, occurring on a kilometer-scale basis, by far the largest source of height uncertainty. To reduce these height errors to 1 m rms, $B_\perp$ would need to exceed 2 km (Eq. (4)), which is still possible to use at L-band.

Figure 4. One-way range delays caused by atmospheric range delays color coded between -3 cm and +3 cm (dark blue to purple, orange, yellow, green and blue), and superimposed on the radar brightness of the terrain.
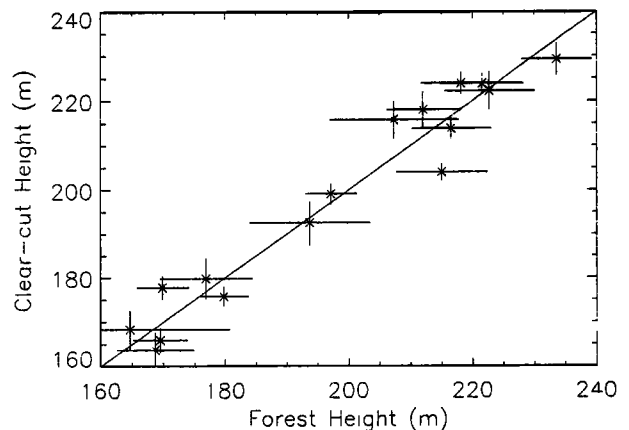

Figure 5. Interferometric height of the forest versus height of adjacent clearings. Horizontal and vertical bars represent the standard deviation of the measurements.

Over areas a few pixels wide, atmospheric delays are uniform and height noise is dominated by phase noise. We compared the height of the forest with the height of adjacent clearings by selecting pairs of 3 x 3 boxes (100 m x 100 m) in forest and non-forest areas, along forest/non-forest transitions, separating the forest box from the non-forest box by 2-3 pixels to avoid possible edge effects. The mean and standard deviation in surface height of each box is plotted for each forest/non-forest pair in Figure 5. We make two observations: 1) the standard deviation in height of the forest is about twice larger than that for cleared areas; and 2) there is little contrast in height between forest and clearings.

The first observation is explained by the higher signal coherence of clearings compared to forests. In the forest, radar signals interact with the canopy volume through multiple interactions which disperse the position of the phase centers along the forest profile.

The second observation suggests the L-band phase centers are located only a few meters above ground. The rms difference in height between the forest and clearings is 5 m, comparable to our estimate of height noise. Our field visit in October 1995 confirmed tree height averages 30 m, with emergent species exceeding 40-50 m and edge effects are not a factor because transitions between forest and clearings occur within 20-30 m.

An airborne radar interferometry / laser altimetry experiment conducted in old-growth forests of the Pacific Northwest indicated the phase centers are a third of the way between the canopy top and the ground at C-band, with large stand-to-stand variability (Rodriguez, personal communication, 1995). At L-band, they should be even closer to the ground. In Rondonia, the phase centers are in the lower 5 m of the forest profile.

Conclusions

Imaging radars operating at long radar wavelengths offer strong and reliable temporal coherence for repeat-pass interferometric applications over vegetated terrain and could measure surface topography beneath thick vegetation canopies. Atmospheric delays however impose that large scale applications of radar interferometry over the humid tropics be conducted either in repeat-pass mode with kilometric baselines, or with two antennas operating simultaneously.

References

Beaudoin A. and 9 others, Retrieval of forest biomass from SAR data, Int. J. Rem. Sens., 15(14), 2777-2796, 1994.

Brown S. and A. Lugo, Above-ground biomass estimates for tropical moist forests of the Brazilian amazon, Interciencia, 17, 201-203, 1992.

Fearnside, P.M., N. Leal and F.M. Fernandes, Rainforest burning and the global carbon budget: biomass, combustion efficiency, and charcoal formation in the Brazilian amazon, J. Geophys. Res., 98, 16,733-16,743, 1993.

Grace, J. and 11 others, Carbon dioxide uptake by an undisturbed tropical rain forest in southwest Amazonia, 1992 to 1993, Science, 270, 778-780.

Goldstein, R.M., Atmospheric limitations to repeat-track radar interferometry, Geophys. Res. Lett., 22, 2517-2520, 1995.

Hagberg, J.O., L. M. H. Ulander, and J. Askne, Repeat-pass SAR interferometry over forested terrain, IEEE Trans. Geosc. Rem. Sens., 33, 331-340, 1995.

Li, F.K. and R.M. Goldstein, Studies of multi-baseline spaceborne interferometric synthetic aperture radars, IEEE Trans. Geosc. Rem. Sens., 28, 88-97, 1990.

Tucker, C.J., B.N. Holben, and T.E. Goff, Intensive forest clearing in Rondonia, Brazil, as detected by satellite remote sensing, Rem. Sens. Environ., 15, 255-261, 1984.

Zebker, H.A. and J. Villasenor, Decorrelation in interferometric radar echoes, IEEE Trans. Geosc. Rem. Sens., 30, 950-959, 1992.

Zebker, H.A., T.G. Farr, R.P. Salaar and T.H. Dixon, Mapping the world's topography using radar interferometry, IEEE Proc., 82, 1774, 1994.

van Beek, L.K.H., Dielectric behavior of heterogeneous systems, Ch. 7 in Progress in Dielectrics, (J. Birks, ed.), Heywood Books, London, 1967.

E. Rignot, Jet Propulsion Laboratory, MS 300-243, California Institute of Technology, 4800 Oak Grove Drive, Pasadena, CA 91109-8099.